Amide proton transfer-weighted magnetic resonance imaging for the diagnosis of symptomatic chronic intracranial artery stenosis: a feasibility study

Kunjian Chen[1,2#^], Weiqiang Dou[3#], Huimin Mao[2], Xinyu Wang[2], Xinyi Wang[1], Yu Guo[2], Chao Zhang[1]

[1]Department of Radiology, The First Affiliated Hospital of Shandong First Medical University & Shandong Provincial Qianfoshan Hospital, Jinan, China; [2]Shandong First Medical University, Jinan, China; [3]Magnetic Resonance Research, GE Healthcare, Beijing, China

Contributions: (I) Conception and design: K Chen, W Dou, H Mao, Xinyi Wang; (II) Administrative support: Xinyi Wang; (III) Provision of study materials or patients: K Chen, W Dou, Xinyu Wang, Y Guo, C Zhang; (IV) Collection and assembly of data: K Chen, W Dou, H Mao, Xinyu Wang; (V) Data analysis and interpretation: K Chen, W Dou, Xinyi Wang; (VI) Manuscript writing: All authors; (VII) Final approval of manuscript: All authors.

[#]These authors contributed equally to this work.

Correspondence to: Xinyi Wang. Department of Radiology, The First Affiliated Hospital of Shandong First Medical University & Shandong Provincial Qianfoshan Hospital, No. 16766 Jingshi Road, Jinan 250014, China. Email: wxy_88@163.com.

Background: Hemodynamic changes after intracranial artery stenosis (ICAS) or occlusion are important causes of metabolic alterations in tissue. This study aimed to explore the feasibility of using amide proton transfer-weighted (APTw) magnetic resonance imaging (MRI) to diagnose patients with symptomatic chronic ICAS based on pH variations caused by metabolite damage.

Methods: Sixty-seven patients with clinically confirmed unilateral anterior circulation ICAS (≥70% arterial narrowing) and 20 healthy volunteers were recruited for the study. Each patient underwent an MRI examination including a T2 fluid-attenuated inversion recovery (T2-FLAIR) sequence, spin-echo echo-planar diffusion-weighted imaging (DWI), three-dimensional pseudo-continuous arterial spin labeling (pcASL), and an APTw sequence. Areas with abnormal perfusion and APTw effects were defined as perfusion/pH matched areas; areas with abnormal perfusion but normal APTw effects were defined as perfusion/pH unmatched areas; the contralateral mirror areas were defined as the normal areas. Regions of interest (ROIs) were selected within these three areas, and the corresponding apparent diffusion coefficient (ADC), cerebral blood flow (CBF), and magnetization transfer ratio asymmetry (MTR_{asym}) were measured.

Results: High intraclass correlation coefficient (ICC) values ($0.78 \leq$ ICCs ≤ 0.97; $P<0.05$) were observed between the two radiologists who independently performed the data analysis. Significant differences were found in CBF and MTR_{asym} between the perfusion/pH matched, perfusion/pH unmatched, and normal areas [$F_{(2,64)}$=288.5, 163.5; both $P<0.05$], but the ADC values were comparable between the three [$F_{(2,64)}$=2.11; $P>0.05$]. Spearman correlation analysis revealed no significant correlation between changes in MTR_{asym} and CBF ($P>0.05$). Finally, APTw showed a robust performance in diagnosing symptomatic chronic ICAS, with an area under the receiver operating characteristic curve (ROC) of 0.953 (sensitivity 97.01%; specificity 85.07%; cut-off value 1.005%).

Conclusions: The present study has demonstrated that metabolic alterations are present in patients with symptomatic chronic ICAS. Our findings illustrate that APTw imaging could potentially serve as an effective method to provide a robust clinical diagnosis for patients with symptomatic chronic ICAS.

^ ORCID: 0000-0003-1749-8848.

Introduction

Intracranial artery stenosis (ICAS) is the primary cause of ischemic events globally. Clinically identified ICAS with a previous transient ischemic attack (TIA) and infarction is known as symptomatic ICAS (1,2). Patients with moderate and severe ischemic stroke are characterized by acute onset, severe symptoms, and high mortality and disability, so these patients have been extensively investigated in previous studies (3,4). In chronic cases, symptomatic ICAS often produces transient or slight neurological deficits (such as recurrent TIA or mild ischemic stroke), and is considered to be an independent predictor of death, a high-risk factor for stroke recurrence, and a priority for secondary prevention (5,6). Therefore, symptomatic chronic ICAS is attracting increasing attention from researchers.

Several imaging modalities have been used to diagnose symptomatic chronic ICAS. Computed tomography (CT) or magnetic resonance imaging (MRI) can reflect morphological changes in brain tissues after infarction. Diffusion-weighted imaging (DWI), a widely applied functional MRI technique for diffusivity measurement in clinic, is particularly sensitive to (sub-)acute ischemic stroke but is prone to misdiagnosing patients with minor stroke in the non-acute stage or TIA (7,8). Magnetic resonance angiography (MRA) and CT angiography (CTA) can display the degree and location of vascular stenosis; however, they are not capable of assessing the state of cerebral parenchymal ischemia (9,10). Also, although perfusion MRI (i.e., perfusion-weighted imaging) can quantitatively measure blood perfusion in tissue and has been proven to have high clinical value in patients with infarction and DWI-negative TIA, this technique frequently overestimates vascular events (11).

Metabolic damage is a key factor for ICAS stroke and may introduce changes before cerebral infarction (12,13). An effective indicator of metabolic alterations caused by hemodynamic changes is pH (14). During ICAS, the body maintains the normal aerobic metabolism through compensatory mechanisms, such as arteriole expansion and collateral circulation opening, and cellular oxygen uptake increases. When stenosis is aggravated, the perfusion pressure decreases beyond its compensatory limit and cell metabolism is damaged, eventually leading to tissue injury and ischemic stroke (15). The pH values of brain tissue change according to the cell's metabolic state after experiencing reduced blood perfusion. Therefore, tissue pH values may be a biological marker of metabolite damage after ischemia (16).

Magnetic resonance spectroscopy (MRS) can measure changes in metabolite concentration in the infarct area and indirectly reflect the pH of brain tissues. However, its clinical application is not wide owing to its intrinsic low resolution and sensitivity (17). As a promising alternative, non-invasive amide proton transfer-weighted (APTw) imaging, which relies on the proton exchange between amide compounds and bulk water, is reportedly sensitive to intracellular pH changes (18,19). For every 0.5 pH unit change in the tissue, the change in the amide proton transfer rate can reach 50–70% (20,21). Because of its high sensitivity to pH variation, APTw imaging has been applied in the diagnosis of (sub-)acute cerebral infarction (22,23). In patients with acute stroke, according to the degree of acidification, the ischemic tissue allows for the stratification of fine tissue damage in the infarct core, ischemic penumbra, and benign hypoperfusion area, which is crucial for revascularization and medical treatment decision-making (24,25). However, whether pH-sensitive APTw imaging can reflect the corresponding changes in metabolism in patients with chronic ICAS has yet to be established.

Therefore, the main goal of this study was to investigate the feasibility of using APTw MRI imaging to diagnose patients with symptomatic chronic ICAS based on pH variations caused by metabolite damage. We present the following article in accordance with the STARD reporting checklist (available at https://qims.amegroups.com/article/view/10.21037/qims-21-1063/rc).

Methods

Patients

The study was conducted in accordance with the

Patients who underwent MRI at our institution with clinical suspicions for symptomatic chronic intracranial artery stenosis from September 2020 to July 2021 (n=246)

Excluded (n=179)
- Posterior circulation severe stenosis (≥70%) or occlusion (n=69)
- Double lateral anterior circulation severe stenosis (≥70%) or occlusion (n=19)
- Acute or subacute cerebral infarction (n=25)
- The interval between the first symptom onset and the examination was <4 weeks (n=32)
- Not underwent APTw imaging (n=12)
- Insufficient image quality (n=16)
- Endovascular therapy for intracranial arterial stenosis before MRI (n=3)
- Hemorrhagic infarction (n=2)
- Concurrent other brain diseases (n=1)

Final enrollment (n=67)

Figure 1 Study population flow diagram. MRI, magnetic resonance imaging; APTw, amide proton transfer-weighted.

Declaration of Helsinki (as revised in 2013). This prospective study was approved by Shandong Province Qianfoshan Hospital Review Board (No. S986), and written informed consent was obtained from all the participants.

Sixty-seven patients were recruited consecutively to the study. They included 41 men and 26 women, aged 56.49±11.27 years old, who were diagnosed with unilateral chronic ICAS (≥70% arterial narrowing) or occlusion by digital subtraction angiography (DSA) or MRA between September 2020 and July 2021 in the Department of Neurology, First Affiliated Hospital of Shandong First Medical University (*Figure 1*). The patient inclusion criteria were as follows: (I) a DSA or MRA diagnosis of unilateral anterior ICAS (≥70% arterial narrowing) or occlusion (including an intracranial segment of the internal carotid artery, middle cerebral artery, and anterior cerebral artery); (II) minor ischemic stroke or TIA, with ischemic symptoms corresponding to the vascular lesion distribution; (III) an interval of ≥4 weeks between the first symptom onset and the examination; and (IV) other intracranial lesions, such as cerebral hemorrhage, were excluded by CT/MRI examination. Patients with the following conditions were excluded: (I) bilateral anterior circulation vascular lesions; (II) complications with severe posterior circulation or extracranial vascular lesions; (III) a large area of acute or subacute infarcts; and (IV) contraindications to MRI examination. Various clinical variables were collected from the patients, including blood pressure and their history of diabetes, smoking, and drinking.

In addition, 20 healthy volunteers (11 men and 9 women, aged 55.40±10.15 years old) were recruited, and their basic clinical data (sex, age, blood pressure, and history of diabetes, smoking, and drinking) were acquired. The lack of stenosis was confirmed by MRA and the lack of obvious abnormalities or the presence of only small lacunar infarcts was confirmed by routine MRI. Further, none of the healthy volunteers had a brain injury or any neurological, psychiatric, metabolic diseases, or other systemic disease that may affect the nervous system.

Acquisition of MRI images

All MRI examinations were performed using a 3.0T MRI scanner (GE Discovery 750, USA) with a 32-channel head coil. In addition to routine MRI imaging [T2 fluid-attenuated inversion recovery (T2-FLAIR) and DWI], three-dimensional pseudo-continuous arterial spin labeling (3D-pcASL) and APTw imaging were performed on each patient. The healthy volunteers only underwent APTw imaging. Two-dimensional fast-spin-echo (FSE)-based T2-FLAIR was first acquired in the axial plane. The scan parameters were as follows: field of view (FOV) =240 mm × 240 mm, slice thickness =5 mm, repetition time (TR)/echo time (TE) =8,000/88.4 ms, inversion time =2,344 ms, matrix size =320×256, number of slices =20, and scanning time =1 min 44 s. A two-dimensional spin-echo echo-planar-imaging (EPI)-based sequence was used for DWI in the axial plane. The scan parameters were as follows: FOV =240 mm × 240 mm, slice thickness =5 mm, TR/TE =3,000/65.6 ms, matrix size =160×160, b=0, 1,000 s/mm^2, number of slices =20, and scan time =24 s. Three-dimensional FSE-based pcASL imaging

was used to measure brain perfusion. The following scan parameters were applied: FOV =240 mm × 240 mm, slice thickness =4 mm, TR/TE =4,632/10.5 ms, matrix size =128×128, labeling time =1,450 ms, post-labeling delay (PLD) =1,525 ms, number of slices =36, and scan time =4 min 29 s. For APTw imaging, a spin-EPI-based sequence was used with three consecutive axial slices centered on the layer of the largest hypoperfusion area for the patients with chronic ICAS and the corresponding three axial slices for the healthy volunteers. B1 saturated images were acquired with 49 off-resonance frequencies ranging from –600 to 600 Hz in increments of 25 Hz, and another three images were acquired at 5,000 Hz but without B1 saturation. The applied saturation B1 power was 2 μT and the saturation duration 2,000 ms. In this study, ±3.5 ppm frequency off sets were acquired, a Fermi shaped radio-frequency pulse was used for chemical exchange saturation transfer (CEST). The other scan parameters were: FOV =240 mm × 240 mm, slice thickness =6 mm, TR/TE =3,000/21.9 ms, matrix size = 128×128, number of slices =3, and total scan time =14 min 15 s.

Data post processing

All data were analyzed using vendor-provided DWI, 3D-pcASL, and APTw post-processing software on the GE workstation 4.6. The apparent diffusion coefficient (ADC) for DWI imaging, 3D-pcASL derived cerebral blood flow (CBF) mapping, and magnetization transfer ratio asymmetry (MTR_{asym}) for APTw imaging were obtained.

The DWI-derived ADC was calculated using the following equation (26):

$$S_b / S_0 = \exp(-b\text{ADC}) \qquad [1]$$

where S_0 is the signal intensity at a b-value of 0, and S_b is the signal intensity at a b value of 1,000 s/mm^2.

The 3D-pcASL-derived CBF mapping was determined by applying the following formula (27):

$$f = \frac{\lambda}{2\alpha T_{1b}\left(1-e^{-\frac{\tau}{T_{1b}}}\right)} \frac{\left(S_{ctrl} - S_{1bl}\right)\left(1-e^{\frac{t_{sat}}{T_{1g}}}\right)}{S_{ref}} e^{\frac{w}{T_{1b}}} \qquad [2]$$

where f is the flow multiplied by a scaling factor [6,000] and converted to physiological units of mL/100 g/min; S is the acquired signal on the control (ctrl), labeled (1bl) signal, or the reference image; T_{1b} and T_{1g} are the T1

values of blood and gray matter, respectively (T_{1b}=1.6 s; T_{1g}=1.2 s); α is the labeling efficiency (α=0.85); λ is the cortex-blood partition coefficient (λ=0.9); and τ and ω represent the labeling duration (1,450 ms) and PLD time (1,525 ms), respectively.

Before generation of the APTw imaging contrast, the B0 map was first calculated with off-resonance frequencies of –200 to 200 Hz based on the water saturation shift reference (WASSR) method (28) for B0 inhomogeneity correction. Then, MTR_{asym} was calculated using the following formula (29):

$$MTR_{asym}\left(\%\right) = \frac{\left(S_{-\Delta\omega} - S_{\Delta\omega}\right)}{S_0} \qquad [3]$$

where $S_{-\Delta\omega}$ and $S_{\Delta\omega}$ correspond to the water signals at negative and positive frequency offsets, respectively, and S_0 is the mean level over three imaging cycles without saturation at 5,000 Hz. To quantify the APTw effect, ω was set to 3.5 ppm.

Regions of interest (ROIs) analysis

Two radiologists (Xinyi Wang and Dong Dong), each with more than 3 years of diagnostic experience in cerebrovascular disease, independently performed the data analysis. CBF and MTR_{asym} images were fused on axial T2-FLAIR images to delineate the abnormal signal area. On the slice with the low perfusion area, areas with abnormal perfusion and APTw effects were defined as perfusion/pH matched areas; areas with abnormal perfusion but normal APTw effects were defined as perfusion/pH unmatched areas; the contralateral mirror areas were the normal areas (*Figure 2*). Three ROIs of comparable area (0.3–0.4 cm^2) were chosen by each radiologist accordingly. These ROIs were further copied onto the ADC, CBF, and MTR_{asym} maps, and the two radiologists obtained the corresponding mean ADC, CBF, and MTR_{asym} values for further statistical analyses.

To investigate the difference in the APTw effect between patients with chronic ICAS and healthy volunteers, 20 of the 67 patients were randomly selected based on the random sampling method using the IBM SPSS 23.0 statistical software (Armonk, NY, USA). Their basic clinical information (sex, age, blood pressure, and their history of diabetes, smoking, and drinking) was matched to that of the 20 healthy volunteers. Because certain differences in APTw effects occur between the left and right cerebral hemispheres in healthy subjects (30), the average APTw effect over the bilateral cerebral hemispheres should be used as a normal reference to exclude the influence of region-specific APTw
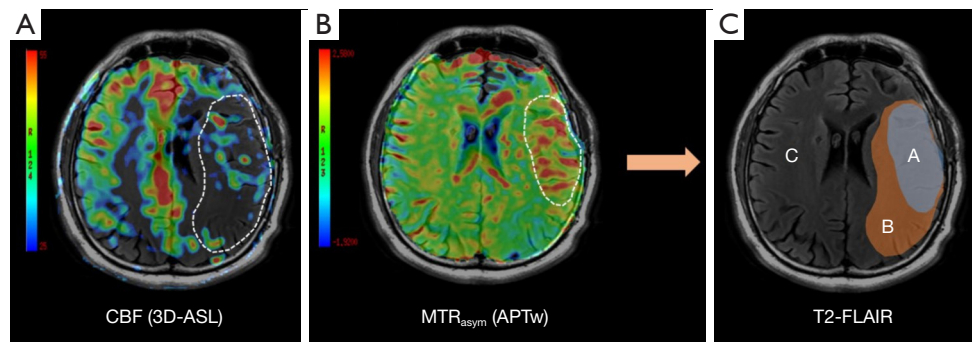
Figure 2 Regional division diagram. (A) CBF and (B) MTR$_{asym}$ images were fused on axial T2-FLAIR images to delineate the abnormal signal area. (C) Axial T2-FLAIR image showing the relationship between CBF and MTR$_{asym}$ abnormal regions. Orange represents abnormal CBF regions; blue represents abnormal MTR$_{asym}$ regions. A shows the perfusion/pH matched region; B shows the perfusion/pH unmatched region; C shows the normal region. CBF, cerebral blood flow; MTR$_{asym}$, magnetization transfer ratio asymmetry; T2-FLAIR, T2 fluid-attenuated inversion recovery sequence.

Table 1 Baseline patient characteristics (n=67)

Variable	Value
Age (mean ± SD) (year)	56.49±11.27
Male/female	41/26
Interval time [median (IQR)] (months)	3 [1–24]
Risk factors, n (%)	
Hypertension	43 (64.18)
Diabetes	15 (22.39)
History of smoking	23 (34.33)
History of drinking	22 (32.84)

SD, standard deviate; IQR, interquartile range.

signals. Therefore, based on the ROIs drawn in the patient group, the bilateral areas in healthy volunteers were selected according to the MTR$_{asym}$ maps, and the mean MTR$_{asym}$ values for both sides were calculated for statistical analysis.

Statistical analysis

All statistical analyses were performed in GraphPad Prism 9 (GraphPad Software, Inc., La Jolla, CA, USA) and IBM SPSS 23.0 (Armonk, NY, USA). The intraclass correlation coefficient (ICC) was used to evaluate the inter-observer agreement for ADC, CBF, and MTR$_{asym}$ measures between the two radiologists, with ICC >0.75 considered to show good reproducibility. The Kolmogorov-Smirnov test was used to test the normality of continuous variables. Continuous variables with normal distribution were expressed as the mean ± standard deviation (SD). A paired t-test was used to compare differences in MTR$_{asym}$ between the healthy volunteers and patients' normal region. One-way analysis of variance (ANOVA) was used to compare differences in ADC, CBF, and MTR$_{asym}$ between the matched, unmatched, and normal regions. A post hoc least-significant difference test was applied to further the compare parameter differences of each group in pairs. Non-normally distributed continuous variables were represented as the median and interquartile range (IQR) and were analyzed using the Wilcoxon rank-sum test. Enumeration data were expressed as n (%) and tested using the χ^2 test. Spearman correlation analysis was used to analyze the correlation between CBF and MTR$_{asym}$ in the matched area. Receiver operating characteristic curve (ROC) analysis and the area under the ROC curve (AUC) were used to evaluate the diagnostic efficacy of APTw-derived MTR$_{asym}$ for symptomatic chronic ICAS. All statistical tests were bilateral, and the significant threshold was set at P<0.05.

Results

Baseline data summary

A total of 67 patients (41 men, aged 53.90±11.98 years old; 26 females, aged 60.19±8.62 years old) were included in our study (*Table 1*). Of the patients, 9 were diagnosed with internal carotid artery lesions, 48 with middle cerebral artery lesions, 1 with an anterior cerebral artery lesion, and 9 with internal carotid artery lesions combined with middle

Table 2 Baseline characteristics and MTR_{asym} of normal brain regions in healthy volunteers and patients with ICAS

Variable	First				Second			
	Patients	Healthy volunteers	t/χ^2	P value	Patients	Healthy volunteers	t/χ^2	P value
Age (mean ± SD) (year)	58.10±10.32	55.40±10.15	0.84	0.41	53.75±12.37	55.40±10.15	0.45	0.66
Male/female	14/6	11/9	0.96	0.33	13/7	11/9	0.42	0.52
Risk factors, n [%]								
Hypertension	13 [65]	10 [50]	0.92	0.34	15 [75]	10 [50]	2.67	0.10
Diabetes	4 [20]	3 [15]	0.17	0.68	3 [15]	3 [15]	0.00	>0.99
History of smoking	9 [45]	8 [40]	0.10	0.75	8 [40]	8 [40]	0.00	>0.99
History of drinking	9 [45]	10 [50]	0.10	0.75	9 [45]	10 [50]	0.10	0.75
MTR_{asym} (mean ± SD) (%)	0.72±0.26	0.68±0.21	0.56	0.59	0.63±0.28	0.64±0.20	0.25	0.81

MTR_{asym}, magnetization transfer ratio asymmetry; ICAS, intracranial artery stenosis.

Table 3 ADC, CBF and MTR_{asym} values in matched, unmatched, and normal areas of patients with ICAS

Variables	Matched area (mean ± SD)	Unmatched area (mean ± SD)	Normal area (mean ± SD)	F	P value
ADC (×10^{-3} mm²/s) (b=1,000 s/mm²)	2.74±0.14	2.69±0.13	2.72±0.13	2.11	0.12
CBF (mL·100 g^{-1}·min^{-1})	20.51±6.68	26.36±6.77	54.79±12.00	288.5	<0.0001
MTR_{asym} (%)	1.38±0.36	0.67±0.19	0.69±0.20	163.5	<0.0001

ADC, apparent diffusion coefficient; CBF, cerebral blood flow; MTR_{asym}, magnetization transfer ratio asymmetry; ICAS, intracranial artery stenosis.

cerebral artery lesions. The ICAS or occlusion etiologies were as follows: thrombus, n=25; atherosclerotic stenosis, n=36; intermural hematoma, n=3; arterial dissection, n=1; and smoke syndrome, n=2. On DWI, 23 patients showed microinfarcts in the disordered vessel supply area, and 44 patients showed no definite infarction lesions with recurrent and intermittent TIA attacks. The median interval from the first ischemic stroke or TIA to the examination was median 3 (IQR 1 to 24) months.

Inter-observer agreement analysis

The ICC analysis revealed high inter-observer agreement between the two radiologists in their measurements of ADC (0.78), CBF (0.95), MTR_{asym} (0.97), and the healthy volunteers' MTR_{asym} (0.93).

Comparison of APTw effects between patients and healthy volunteers

Twenty patients (first: 14 male/6 female, aged 58.10±10.32 years old; second: 13 male/7 female, aged

53.75±12.37 years old) were randomly selected and compared with 20 healthy volunteers (11 male/9 female, aged 55.40±10.15 years old). The χ^2 test showed no significant difference in baseline characteristics between the patients and the healthy volunteers (P>0.05). Using paired *t*-test analysis, the MTR_{asym} of the contralateral normal region of randomly selected patients was comparable with the mean MTR_{asym} of the bilateral brain parenchyma of the healthy controls (P>0.05; *Table 2*).

Quantitative analysis of DWI, 3D-pcASL and APTw imaging of patients with ICAS

One-way ANOVA revealed significant differences in the CBF and MTR_{asym} values between the perfusion/pH matched, unmatched, and normal areas [$F_{(2,64)}$=288.5, 163.5; both P<0.0001]; however, the ADC values were comparable between the areas [mean: (2.74±0.14)×10^{-3} *vs.* (2.69±0.13)×10^{-3} *vs.* (2.72±0.13)×10^{-3} mm²/s, $F_{(2,64)}$=2.11, P>0.05; *Table 3*]. In the further post hoc least-significant difference test, the matched side showed significantly lower CBF (20.51±6.68 mL·100 g^{-1}·min^{-1}) than the
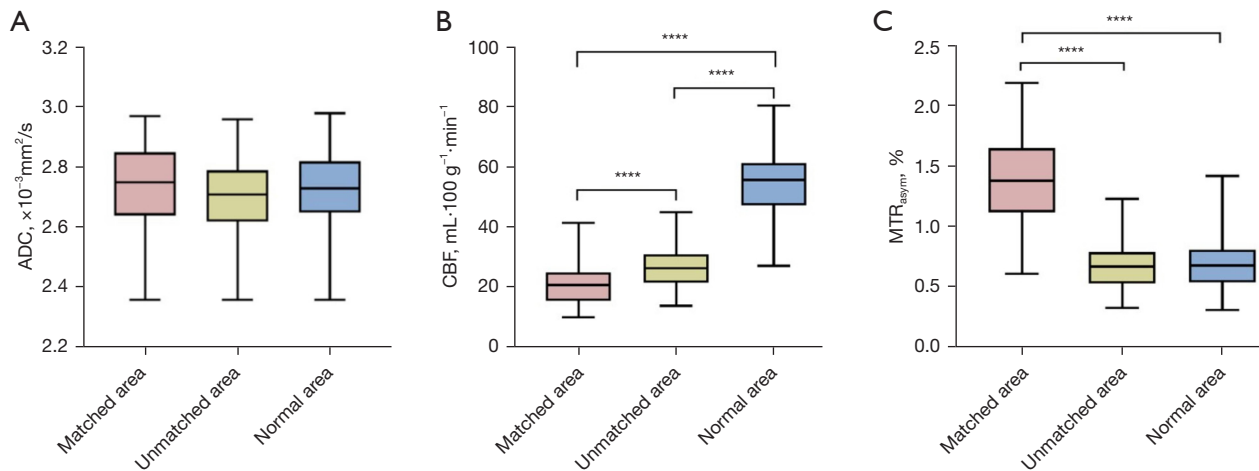
Figure 3 Box-plot analysis. Group comparisons of (A) ADC, (B) CBF, and (C) MTR$_{asym}$ among matched, unmatched, and normal areas using box-plot analysis (significant difference: ****, P<0.0001). Areas with abnormal perfusion and APTw effects were defined as perfusion/pH matched areas; areas with abnormal perfusion but normal APTw effects were defined as perfusion/pH unmatched areas; the contralateral mirror areas were defined as the normal areas. ADC, apparent diffusion coefficient; CBF, cerebral blood flow; MTR$_{asym}$, magnetization transfer ratio asymmetry; APTw, amide proton transfer-weighted.

unmatched side (26.36±6.77 mL·100 g^{-1}·min^{-1}) and the contralateral side (54.79±12.00 mL·100 g^{-1}·min^{-1}; all P<0.0001). Higher MTR$_{asym}$ was found in the matched side (1.38%±0.36%) than in the unmatched (0.67%±0.19%) and contralateral (0.69%±0.20%) sides (all P<0.0001). However, the difference between the unmatched and contralateral sides was not statistically significant (P=0.89; *Figure 3*).

Correlation analysis between CBF and MTRasym in the matched areas of patients with ICAS

Spearman correlation analysis was applied to investigate the relationship between CBF and MTR$_{asym}$ changes in the perfusion/pH matched region in patients with ICAS. No significant correlation was found between the changes in CBF and MTR$_{asym}$ (CBF and MTR$_{asym}$, r=−0.14, P=0.26; CBF$_{(/normal-matched/)}$ and MTR$_{asym\,(/normal-matched/)}$, r=0.03, P=0.81; CBF$_{(normal/matched)}$ and MTR$_{asym(normal/matched)}$, r=−0.03, P=0.78; *Figure 4*).

Diagnostic ROC analysis of APTw imaging for symptomatic chronic ICAS

The ROC analysis confirmed the robust clinical efficacy of APTw-derived MTR$_{asym}$ for diagnosing symptomatic chronic ICAS, with a high AUC (0.953) and sensitivity and

specificity of 97.01% and 85.07%, respectively (*Figure 5*). The cut-off MTR$_{asym}$ value was 1.005%.

Discussion

This study investigated the clinical value of using intracellular pH-sensitive APTw imaging to reflect metabolite damage-induced pH variation in chronic ischemic brain tissues for the diagnosis of patients with symptomatic chronic ICAS. The intracranial arteries mainly include the anterior and posterior circulation systems. Bilateral cerebral hemispheres are mainly supplied by the anterior circulation, specifically the middle cerebral artery. Therefore, in this study, we chose patients with unilateral anterior circulation artery stenosis or occlusion. Aside from DWI and 3D-pcASL, we performed APTw imaging to measure the hypoperfusion area of brain tissues caused by unilateral anterior circulation artery stenosis or occlusion. The resultant ADC, CBF, and MTR$_{asym}$ were quantitatively compared between the affected and normal sides to analyze the chronic ischemic tissues further. We found no abnormal ADC in the matched, unmatched, and normal areas of patients, but abnormal CBF and MTR$_{asym}$ levels were found in diseased vessels.

Interestingly, the abnormal CBF and MTR$_{asym}$ areas were not perfectly matched. In the matched area, CBF decreased, and MTR$_{asym}$ increased, but no significant correlation was
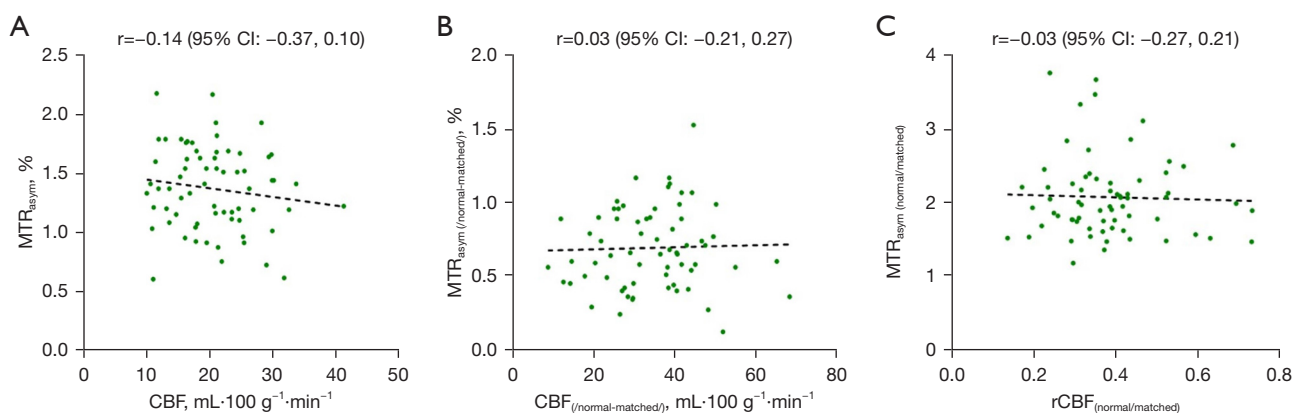
Figure 4 Spearman correlation analysis. Spearman correlation analysis between changes in (A) CBF and MTR_{asym}, (B) $CBF_{(/normal-matched/)}$ and $MTR_{asym(/normal-matched/)}$, and (C) $CBF_{(normal/matched)}$ and $MTR_{asym(normal/matched)}$. $MTR_{asym(/normal-matched/)}$: the absolute difference in MTR_{asym} between the normal side and the perfusion/pH matched area. $MTR_{asym\,(normal/matched)}$: MTR_{asym} ratio of normal side to perfusion/pH matched area. $CBF_{(/normal-matched/)}$: the absolute difference in CBF between the normal side and the perfusion/pH matched area. $CBF_{(normal/matched)}$: CBF ratio of normal side to perfusion/pH matched area). CBF, cerebral blood flow; MTR_{asym}, magnetization transfer ratio asymmetry.
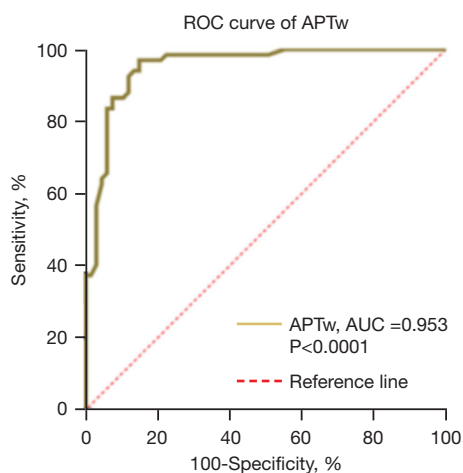
Figure 5 Using ROC curve analysis, APTw-derived MTR_{asym} showed a robust performance in diagnosing symptomatic chronic ICAS, with a high AUC of 0.953, sensitivity of 97.01%, and specificity of 85.07%. The corresponding MTR_{asym} cut-off value was 1.005%. ROC, receiver operating characteristic; APTw, amide proton transfer-weighted; AUC, area under curve; MTR_{asym}, magnetization transfer ratio asymmetry; ICAS, intracranial artery stenosis.

found between the changes in CBF and MTR_{asym}. In the unmatched area, CBF also decreased, but MTR_{asym} in this area was not statistically different from that in the normal area (*Figure 6*). Further, ROC analysis demonstrated the robust performance of APTw imaging in diagnosing symptomatic chronic ICAS, with high AUC, sensitivity, and specificity values.

In our study, tissue perfusion in the affected side was obviously reduced compared with that in the contralateral region, and APTw imaging in partial hypoperfusion areas (perfusion/pH matched regions) showed a high signal. In ischemic disease, Zhou *et al.* (19) showed that the exchange rate of amide protons was highly sensitive to pH changes. The significant change in the high APTw signal in our study could be attributed to the elevated pH level in the lesion. Sappey-Marinier *et al.* (31) showed that, for patients with chronic ischemic stroke, the pH was higher in the stroke group than in the control group (7.25±0.07 *vs.* 7.03±0.04). A recent study by Seiler *et al.* (32) found that, before the carotid intervention, T2' was significantly decreased in hypoperfusion areas ipsilateral to the stenosis relative to the contralateral side, and intracellular pH and T2' showed a significant negative relationship. With these findings, it can be speculated that the pH levels in hypoperfusion areas ipsilateral to the stenosis are increased, which was consistent with our results. However, the mechanism of tissue alkalosis in the brain after hypoxia-ischemia has not been fully elucidated. Studies in the literature tend to agree that this phenomenon is caused by an active compensatory mechanism after tissue acidosis or a relatively high perfusion state after necrosis (33,34).

In this study, a simple index of MTR_{asym}, which has been widely applied in clinical CEST studies, was calculated to assess the APT effect quantitatively. However, in addition
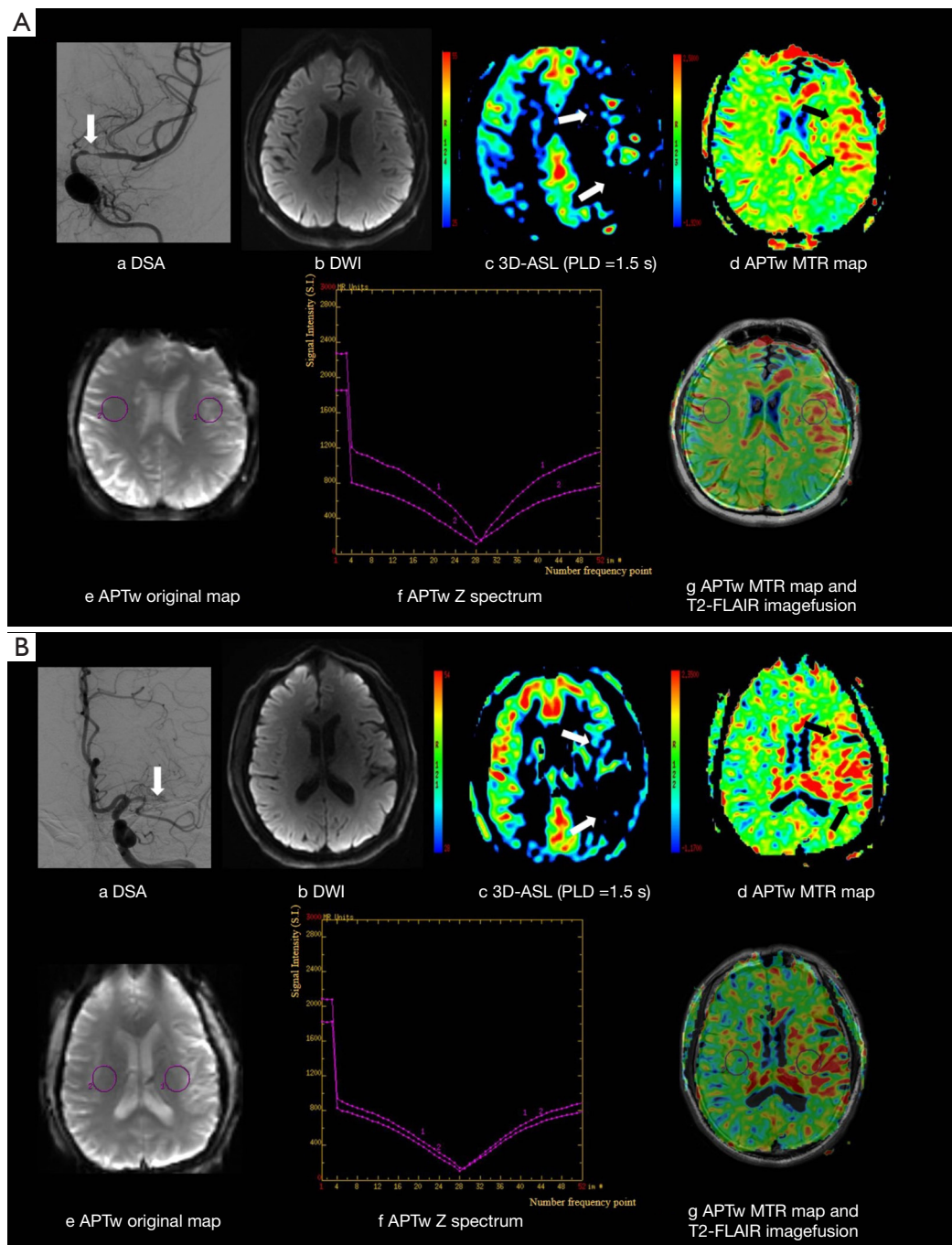
Figure 6 Typical cases. (A) A 49-year-old man with severe stenosis of the left MCA M1. (B) A 56-year-old man with an occlusion in the left MCA [a, white arrow; b, DWI (b=1,000 s/mm^2)] showed no obvious abnormal signals. (c) Lower perfusion in the ipsilateral side than in the contralateral side; A-CBF$_{ave}$ =20.48 *vs.* 38.16 mL·100 g^{-1}·min^{-1}; B-CBF$_{ave}$ =19.32 *vs.* 40.72 mL·100 g^{-1}·min^{-1} (white arrows). (d) High APTw value area; A-MTR$_{asym}$ =1.41% *vs.* 0.68%; B-MTR$_{asym}$ =1.47% *vs.* 0.54% (black arrows). (e) APTw original map; (f) APTw Z spectrum, MR units represent signal intensity, images (im) represent the corresponding number frequency point; (g) APTw MTR map and T2-FLAIR image fusion. DSA, digital subtraction angiography; DWI, diffusion-weighted imaging; 3D-ALS, three-dimensional arterial spin labeling; PLD, post-labeling delay; APTw, amide proton transfer-weighted; MTR, magnetization transfer ratio; T2-FLAIR, T2 fluid-attenuated inversion recovery sequence; MCA, middle cerebral artery; CBF, cerebral blood flow; MTR$_{asym}$, magnetization transfer ratio asymmetry.

to the pure APT effect, other components, including magnetization transfer (MT), direct saturation (DS) as well as relayed nuclear Overhauser enhancement (rNOE), may also contribute to MTR_{asym} at 3.5 ppm, and the effect of rNOE is sensitive to intracellular pH level (35). Nowadays, multiple advanced post-processing methods for CEST effect analysis have been developed to separate pure APT signals from other signals. A novel method called extrapolated semisolid MT reference can remove the rNOE signal and obtain the APT signal (36). Another apparent exchange-dependent relaxation method takes into account the contribution of the T1 relaxation time while quantifying the CEST effect (37). With these advantages, our follow-up study may investigate the relationship between pH variation and the APT effect in the hypoperfusion areas of patients with symptomatic chronic ICAS.

Neither pH nor metabolite levels were measured directly in our study. Mapping pH based on CEST could provide a quantitative pH level for the abnormal metabolic region. Based on analysis of CEST effects under different radio frequency irradiation power levels (38), a novel ratiometric pH MRI method has been proposed to generate pH mapping that can be used for glioma pH quantification, skeletal muscle, and renal pH mapping (39-41). We will consider the application of pH mapping in our follow-up study.

Compared with previous MRS studies on metabolic changes in chronic cerebral infarction, our study did not find obvious signs of infarction in ADC maps. This result may be due to small and scattered ischemic infarction cells in the hypoperfusion area when no marked lesions had yet formed. A previous ^{1}H-MRS study (42) found that N-acetyl aspartate decreased and choline increased in the brain tissues of patients with a non-infarcted internal carotid artery, middle cerebral artery severe stenosis or occlusion. The results confirmed the presence of brain cell damage in non-infarcted areas. In acute ischemic stroke studies, the APTw/DWI mismatch zone around the infarct core, known as the ischemic penumbra, was key to clinical treatment and prognosis (43-45). Accordingly, we speculate that tissues in the abnormal pH region might have metabolic and electrophysiological abnormalities but are not yet dead, which can survive or progress to complete necrosis. However, the specific mechanism underlying these findings needs to be further validated. Nevertheless, these tissues with metabolic abnormalities may be a potential cause of ischemic stroke symptoms and may increase the risk of ischemic stroke.

Lower tissue perfusion is the fundamental reason for changes in the cellular pH level. The APTw signal intensity has been reported to reflect the pH-weighted characteristics of ischemic tissue at different stages or time points (23,44). Therefore, we evaluated the relationship between CBF and MTR_{asym} changes in the perfusion/pH matched region. However, no significant correlation was observed. A previous study showed that although a decrease in CBF caused a change in the tissue pH, the tissue pH did not change with the CBF after ischemia, which may be related to the dynamic change in the tissue pH value with the extension of ischemia time (16). In the early stage of ischemic injury, different processes occur in the affected brain tissues, including a sharp decrease in blood flow, insufficient tissue perfusion, aerobic metabolic disorder, increased anaerobic metabolism, and lactic acid accumulation. These events eventually lead to a decrease in pH. Low pH in cells may cause tissue damage by activating destructive enzymes such as proteases and lipases (12). Previous APTw and MRS studies (46-48) have confirmed an increase in lactic acid, a decrease in MTR_{asym}, and neuron damage in the acute infarction area. With the increase in the ischemic injury time, the acidification gradually eased and the pH increased. Zöllner *et al.* (33) showed that the pH of subacute stroke tissue was significantly increased compared to that of the contralateral healthy tissue. Song *et al.* (23) reflected the dynamic pH evolution in post-infarction tissue by grouping stroke patients according to onset time. Also, alkalosis in the later stage of metabolic tissue injury is related to various mechanisms, and tissue sensitivity to ischemia differs. Therefore, we were unable to establish a clear correlation between CBF and MTR_{asym} changes.

In this study, we found that the hypoperfusion area was larger than the APTw hyperintensity area on the lesion side (the perfusion/pH unmatched area). In acute ischemic infarction studies, similar mismatched areas have been called "benign hypoperfusion areas" (24,25). The progression from hemodynamic damage to metabolic alterations can be divided into three stages: 0, I, and II (15). In stage 0, the cerebral vessels maintain a constant CBF through small artery self-regulation. With a further decrease in perfusion pressure, CBF starts to decrease when it exceeds the autoregulation limit of vasodilation. In stage I, brain cells begin to obtain enough oxygen to maintain their own physiological and metabolic needs by increasing the oxygen extraction fraction. Positron emission tomography and quantitative susceptibility mapping (QSM) studies have confirmed

the existence of this compensatory process (49-52). In addition, the collateral circulation pathway in the brain gradually opens, providing an alternative vascular pathway for ischemic tissue (53,54). In stage II, the body's reserve capacity is exhausted, and the ischemic tissue shows metabolic alterations and changes in pH. In severe cases, ischemic stroke eventually occurs. Therefore, despite the fluctuating cerebral perfusion and oxygen saturation in the perfusion/pH unmatched area, the tissue pH is well regulated under normal physiological conditions and the APTw signal is at a normal level.

Currently, angiography imaging techniques such as CTA, MRA, or DSA are widely used in the clinical diagnosis of ICAS or occlusion. In recent years, high-resolution vascular wall MRI, with its unique imaging mode, has gradually demonstrated its diagnostic value in assessing stenosis etiology and predicting stroke risk (55,56). However, the damage to the blood flow rate is not necessarily related to the degree of arterial stenosis, and collateral connections and compensation mechanisms between cerebral arteries play an important role (57,58). Compared with these imaging methods, perfusion imaging, such as 3D-pcASL, can more directly and sensitively reflect hemodynamic changes in cerebral artery stenosis or occlusion. However, in patients with severe chronic ICAS, 3D-pcASL may overestimate the size of the hypoperfused area due to the slow compensatory blood flow (59,60). However, APTw can exclude the influence of compensatory factors and directly reflect tissue metabolism damage. Our experimental results confirm that APTw has high diagnostic efficiency for ICAS. Therefore, APTw can provide added clinical diagnostic value in new dimensions from the perspective of molecular biology.

Limitations

Our study has several limitations. First, our study had a limited sample size, which may have introduced potential selection bias. Second, due to technical and time constraints, we did not perform APTw imaging in more than three slices covering the whole blood supply area for the narrowed artery. Third, we did not include patients with posterior circulatory artery stenosis because the APTw signal has been reported to have poor reproducibility in the subtentorial position (61).

Conclusions

High APTw-derived MTR_{asym} could reflect pH variation

in patients with symptomatic chronic ICAS, which may indicate the presence of potential metabolic alterations in brain tissues in chronic ischemia. Therefore, APTw imaging may be an effective method to provide a new dimension and additional clinical value in the diagnosis of patients with symptomatic chronic ICAS.

Acknowledgments

Footnote

Conflicts of Interest: All authors have completed the ICMJE uniform disclosure form (available at https://qims. amegroups.com/article/view/10.21037/qims-21-1063/coif). All the authors report that this work was supported by the Science and Technology Development Plan Contract of Shandong Province (No. 2009GG10002024). And WD is an employee of GE Healthcare. The authors have no other conflicts of interest to declare.

Ethical Statement: The authors are accountable for all aspects of the work in ensuring that questions related to the accuracy or integrity of any part of the work are appropriately investigated and resolved. The study was conducted in accordance with the Declaration of Helsinki (as revised in 2013). This prospective study was approved by the Shandong Province Qianfoshan Hospital Review Board (No. S986), and written informed consent was obtained from all patients.

References

1. Ryu WS, Park SS, Kim YS, Lee SH, Kang K, Kim C, Sohn CH, Lee SH, Yoon BW. Long-term natural history of intracranial arterial stenosis: an MRA follow-up study. Cerebrovasc Dis 2014;38:290-6.

2. Lan L, Leng X, Abrigo J, Ip V, Soo YO, Leung T, Chen X, Wong KS. Cerebral perfusion difference between hemispheres with symptomatic and asymptomatic intracranial arterial stenosis. Int J Stroke 2017;12:NP19-20.

3. Johnson W, Onuma O, Owolabi M, Sachdev S. Stroke: a global response is needed. Bull World Health Organ 2016;94:634-634A.

4. Wang YZ, Zhang HY, Liu F, Li L, Deng SM, He ZY. Association between PPARG genetic polymorphisms and ischemic stroke risk in a northern Chinese Han population: a case-control study. Neural Regen Res 2019;14:1986-93.

5. Reeves M, Khoury J, Alwell K, Moomaw C, Flaherty M, Woo D, Khatri P, Adeoye O, Ferioli S, Kissela B, Kleindorfer D. Distribution of National Institutes of Health stroke scale in the Cincinnati/Northern Kentucky Stroke Study. Stroke 2013;44:3211-3.

6. Wang Y, Li Z, Wang Y, Zhao X, Liu L, Yang X, Wang C, Gu H, Zhang F, Wang C, Xian Y, Wang DZ, Dong Q, Xu A, Zhao J. Chinese Stroke Center Alliance: a national effort to improve healthcare quality for acute stroke and transient ischaemic attack: rationale, design and preliminary findings. Stroke Vasc Neurol 2018;3:256-62.

7. Lin MP, Liebeskind DS. Imaging of Ischemic Stroke. Continuum (Minneap Minn) 2016;22:1399-423.

8. El-Koussy M, Schroth G, Brekenfeld C, Arnold M. Imaging of acute ischemic stroke. Eur Neurol 2014;72:309-16.

9. Baradaran H, Patel P, Gialdini G, Al-Dasuqi K, Giambrone A, Kamel H, Gupta A. Quantifying Intracranial Internal Carotid Artery Stenosis on MR Angiography. AJNR Am J Neuroradiol 2017;38:986-90.

10. Josephson SA, Bryant SO, Mak HK, Johnston SC, Dillon WP, Smith WS. Evaluation of carotid stenosis using CT angiography in the initial evaluation of stroke and TIA. Neurology 2004;63:457-60.

11. Lee SH, Nah HW, Kim BJ, Ahn SH, Kim JS, Kang DW, Kwon SU. Role of Perfusion-Weighted Imaging in a Diffusion-Weighted-Imaging-Negative Transient Ischemic Attack. J Clin Neurol 2017;13:129-37.

12. Siesjö BK, Ekholm A, Katsura K, Theander S. Acid-base changes during complete brain ischemia. Stroke 1990;21:III194-9.

13. Hossmann KA. Viability thresholds and the penumbra of focal ischemia. Ann Neurol 1994;36:557-65.

14. Leigh R, Knutsson L, Zhou J, van Zijl PC. Imaging the physiological evolution of the ischemic penumbra in acute ischemic stroke. J Cereb Blood Flow Metab 2018;38:1500-16.

15. Grubb RL Jr, Derdeyn CP, Fritsch SM, Carpenter DA, Yundt KD, Videen TO, Spitznagel EL, Powers WJ. Importance of hemodynamic factors in the prognosis of symptomatic carotid occlusion. JAMA 1998;280:1055-60.

16. Orlowski P, Chappell M, Park CS, Grau V, Payne S. Modelling of pH dynamics in brain cells after stroke. Interface Focus 2011;1:408-16.

17. Houkin K, Kamada K, Kamiyama H, Iwasaki Y, Abe H, Kashiwaba T. Longitudinal changes in proton magnetic resonance spectroscopy in cerebral infarction. Stroke 1993;24:1316-21.

18. Zhou J, Wilson DA, Sun PZ, Klaus JA, Van Zijl PC. Quantitative description of proton exchange processes between water and endogenous and exogenous agents for WEX, CEST, and APT experiments. Magn Reson Med 2004;51:945-52.

19. Zhou J, Payen JF, Wilson DA, Traystman RJ, van Zijl PC. Using the amide proton signals of intracellular proteins and peptides to detect pH effects in MRI. Nat Med 2003;9:1085-90.

20. Zhou J, van Zijl PC. Defining an Acidosis-Based Ischemic Penumbra from pH-Weighted MRI. Transl Stroke Res 2011;3:76-83.

21. Sun PZ, Benner T, Copen WA, Sorensen AG. Early experience of translating pH-weighted MRI to image human subjects at 3 Tesla. Stroke 2010;41:S147-51.

22. Sun PZ, Zhou J, Sun W, Huang J, van Zijl PC. Detection of the ischemic penumbra using pH-weighted MRI. J Cereb Blood Flow Metab 2007;27:1129-36.

23. Song G, Li C, Luo X, Zhao X, Zhang S, Zhang Y, Jiang S, Wang X, Chen Y, Chen H, Gong T, Zhou J, Chen M. Evolution of Cerebral Ischemia Assessed by Amide Proton Transfer-Weighted MRI. Front Neurol 2017;8:67.

24. Guo Y, Zhou IY, Chan ST, Wang Y, Mandeville ET, Igarashi T, Lo EH, Ji X, Sun PZ. pH-sensitive MRI demarcates graded tissue acidification during acute stroke - pH specificity enhancement with magnetization transfer and relaxation-normalized amide proton transfer (APT) MRI. Neuroimage 2016;141:242-9.

25. Wang E, Wu Y, Cheung JS, Igarashi T, Wu L, Zhang X, Sun PZ. Mapping tissue pH in an experimental model of acute stroke - Determination of graded regional tissue

5196

Chen et al. APTw MRI for symptomatic chronic ICAS diagnosis

pH changes with non-invasive quantitative amide proton transfer MRI. Neuroimage 2019;191:610-7.

26. Zhang SX, Jia QJ, Zhang ZP, Liang CH, Chen WB, Qiu QH, Li H. Intravoxel incoherent motion MRI: emerging applications for nasopharyngeal carcinoma at the primary site. Eur Radiol 2014;24:1998-2004.

27. Wang X, Dou W, Dong D, Wang X, Chen X, Chen K, Mao H, Guo Y, Zhang C. Can 3D Pseudo-Continuous Territorial Arterial Spin Labeling Effectively Diagnose Patients With Recanalization of Unilateral Middle Cerebral Artery Stenosis? J Magn Reson Imaging 2021;54:175-83.

28. Kim M, Gillen J, Landman BA, Zhou J, van Zijl PC. Water saturation shift referencing (WASSR) for chemical exchange saturation transfer (CEST) experiments. Magn Reson Med 2009;61:1441-50.

29. Dou W, Lin CE, Ding H, Shen Y, Dou C, Qian L, Wen B, Wu B. Chemical exchange saturation transfer magnetic resonance imaging and its main and potential applications in pre-clinical and clinical studies. Quant Imaging Med Surg 2019;9:1747-66.

30. Sartoretti T, Sartoretti E, Wyss M, Schwenk Á, Najafi A, Binkert C, Reischauer C, Zhou J, Jiang S, Becker AS, Sartoretti-Schefer S. Amide Proton Transfer Contrast Distribution in Different Brain Regions in Young Healthy Subjects. Front Neurosci 2019;13:520.

31. Sappey-Marinier D, Hubesch B, Matson GB, Weiner MW. Decreased phosphorus metabolite concentrations and alkalosis in chronic cerebral infarction. Radiology 1992;182:29-34.

32. Seiler A, Kammerer S, Gühl A, Schüre JR, Deichmann R, Nöth U, Pfeilschifter W, Hattingen E, Keese M, Pilatus U, Wagner M. Revascularization of High-Grade Carotid Stenosis Restores Global Cerebral Energy Metabolism. Stroke 2019;50:1742-50.

33. Zöllner JP, Hattingen E, Singer OC, Pilatus U. Changes of pH and energy state in subacute human ischemia assessed by multinuclear magnetic resonance spectroscopy. Stroke 2015;46:441-6.

34. Sappey-Marinier D, Calabrese G, Hetherington HP, Fisher SN, Deicken R, Van Dyke C, Fein G, Weiner MW. Proton magnetic resonance spectroscopy of human brain: applications to normal white matter, chronic infarction, and MRI white matter signal hyperintensities. Magn Reson Med 1992;26:313-27.

35. Zhou J, Heo HY, Knutsson L, van Zijl PCM, Jiang S. APT-weighted MRI: Techniques, current neuro applications, and challenging issues. J Magn Reson

Imaging 2019;50:347-64.

36. Heo HY, Zhang Y, Jiang S, Lee DH, Zhou J. Quantitative assessment of amide proton transfer (APT) and nuclear overhauser enhancement (NOE) imaging with extrapolated semisolid magnetization transfer reference (EMR) signals: II. Comparison of three EMR models and application to human brain glioma at 3 Tesla. Magn Reson Med 2016;75:1630-9.

37. Zaiss M, Xu J, Goerke S, Khan IS, Singer RJ, Gore JC, Gochberg DF, Bachert P. Inverse Z-spectrum analysis for spillover-, MT-, and T1 -corrected steady-state pulsed CEST-MRI--application to pH-weighted MRI of acute stroke. NMR Biomed 2014;27:240-52.

38. Longo DL, Sun PZ, Consolino L, Michelotti FC, Uggeri F, Aime S. A general MRI-CEST ratiometric approach for pH imaging: demonstration of in vivo pH mapping with iobitridol. J Am Chem Soc 2014;136:14333-6.

39. Ferrauto G, Di Gregorio E, Auboiroux V, Petit M, Berger F, Aime S, Lahrech H. CEST-MRI for glioma pH quantification in mouse model: Validation by immunohistochemistry. NMR Biomed 2018;31:e4005.

40. Chen YW, Liu HQ, Wu Q, Huang YH, Tung YY, Lin MH, Lin CH, Chen TC, Lin EC, Hwang DW. pH Mapping of Skeletal Muscle by Chemical Exchange Saturation Transfer (CEST) Imaging. Cells 2020;9:2610.

41. Pavuluri KD, Consolino L, Longo DL, Irrera P, Sun PZ, McMahon MT. Renal pH Mapping Using Chemical Exchange Saturation Transfer (CEST) MRI: Experimental Protocol. Methods Mol Biol 2021;2216:455-71.

42. Zhang M, Lu J, Jiao L, Ma Q, Li K. Proton magnetic resonance spectroscopy in patients with symptomatic unilateral internal carotid artery / middle cerebral artery stenosis or occlusion. J Magn Reson Imaging 2011;34:910-6.

43. Tietze A, Blicher J, Mikkelsen IK, Østergaard L, Strother MK, Smith SA, Donahue MJ. Assessment of ischemic penumbra in patients with hyperacute stroke using amide proton transfer (APT) chemical exchange saturation transfer (CEST) MRI. NMR Biomed 2014;27:163-74.

44. Jokivarsi KT, Gröhn HI, Gröhn OH, Kauppinen RA. Proton transfer ratio, lactate, and intracellular pH in acute cerebral ischemia. Magn Reson Med 2007;57:647-53.

45. Davis S, Donnan GA. Time is Penumbra: imaging, selection and outcome. The Johann jacob wepfer award 2014. Cerebrovasc Dis 2014;38:59-72.

46. Lepore MG, Buscemi L, Hirt L, Lei H. Metabolic fingerprints discriminating severity of acute ischemia using in vivo high-field 1 H magnetic resonance spectroscopy. J

Neurochem 2020;152:252-62.

47. Qian J, Qian B, Lei H. Reversible loss of N-acetylaspartate after 15-min transient middle cerebral artery occlusion in rat: a longitudinal study with in vivo proton magnetic resonance spectroscopy. Neurochem Res 2013;38:208-17.

48. Sun PZ, Cheung JS, Wang E, Lo EH. Association between pH-weighted endogenous amide proton chemical exchange saturation transfer MRI and tissue lactic acidosis during acute ischemic stroke. J Cereb Blood Flow Metab 2011;31:1743-50.

49. Kudo K, Liu T, Murakami T, Goodwin J, Uwano I, Yamashita F, Higuchi S, Wang Y, Ogasawara K, Ogawa A, Sasaki M. Oxygen extraction fraction measurement using quantitative susceptibility mapping: Comparison with positron emission tomography. J Cereb Blood Flow Metab 2016;36:1424-33.

50. Liu Z, Li Y. Cortical Cerebral Blood Flow, Oxygen Extraction Fraction, and Metabolic Rate in Patients with Middle Cerebral Artery Stenosis or Acute Stroke. AJNR Am J Neuroradiol 2016;37:607-14.

51. Zhang J, Liu T, Gupta A, Spincemaille P, Nguyen TD, Wang Y. Quantitative mapping of cerebral metabolic rate of oxygen (CMRO2) using quantitative susceptibility mapping (QSM). Magn Reson Med 2015;74:945-52.

52. Uwano I, Kudo K, Sato R, Ogasawara K, Kameda H, Nomura JI, Mori F, Yamashita F, Ito K, Yoshioka K, Sasaki M. Noninvasive Assessment of Oxygen Extraction Fraction in Chronic Ischemia Using Quantitative Susceptibility Mapping at 7 Tesla. Stroke 2017;48:2136-41.

53. Ramakrishnan G, Dong B, Todd KG, Shuaib A, Winship IR. Transient Aortic Occlusion Augments Collateral Blood Flow and Reduces Mortality During Severe Ischemia due to Proximal Middle Cerebral Artery Occlusion. Transl Stroke Res 2016;7:149-55.

54. Wufuer A, Mijiti P, Abudusalamu R, Dengfeng H, Jian C, Jianhua M, Xiaoning Z. Blood pressure and collateral circulation in acute ischemic stroke. Herz 2019;44:455-9.

55. Natori T, Sasaki M, Miyoshi M, Ito K, Ohba H, Miyazawa H, Narumi S, Kabasawa H, Harada T, Terayama Y. Intracranial Plaque Characterization in Patients with Acute Ischemic Stroke Using Pre- and Post-Contrast Three-Dimensional Magnetic Resonance Vessel Wall Imaging. J Stroke Cerebrovasc Dis 2016;25:1425-30.

56. Meng Y, Li M, Yu Y, Xu Y, Gao S, Feng F, Xu WH. Quantitative score of the vessel morphology in middle cerebral artery atherosclerosis. J Neurol Sci 2019;399:111-7.

57. Zhuang C, Poublanc J, Mcketton L, Venkatraghavan L, Sobczyk O, Duffin J, Crawley AP, Fisher JA, Wu R, Mikulis DJ. The value of a shorter-delay arterial spin labeling protocol for detecting cerebrovascular impairment. Quant Imaging Med Surg 2021;11:608-19.

58. Zarrinkoob L, Wåhlin A, Ambarki K, Birgander R, Eklund A, Malm J. Blood Flow Lateralization and Collateral Compensatory Mechanisms in Patients With Carotid Artery Stenosis. Stroke 2019;50:1081-8.

59. Bivard A, Krishnamurthy V, Stanwell P, Levi C, Spratt NJ, Davis S, Parsons M. Arterial spin labeling versus bolus-tracking perfusion in hyperacute stroke. Stroke 2014;45:127-33.

60. Tian B, Liu Q, Wang X, Chen S, Xu B, Zhu C, Lu J. Chronic intracranial artery stenosis: Comparison of whole-brain arterial spin labeling with CT perfusion. Clin Imaging 2018;52:252-9.

61. Lee JB, Park JE, Jung SC, Jo Y, Kim D, Kim HS, Choi CG, Kim SJ, Kang DW. Repeatability of amide proton transfer-weighted signals in the brain according to clinical condition and anatomical location. Eur Radiol 2020;30:346-56.